Transverse energy measurements with ALICE

Christine Nattrass (UTK) for the ALICE collaboration

The ALICE detector allows precise measurements of the transverse energy at LHC energies. We discuss studies of the transverse energy in Pb–Pb collisions at $\sqrt{s_{NN}}$ = 2.76 TeV. The ALICE Inner Tracking System (ITS) and the Time Projection Chamber (TPC) are used for precise measurements of the transverse energy of charged hadrons. The detector performance and the measurement technique are described in detail with particular focus on Monte Carlo studies and the assignment of systematic errors for the hadronic E_{T}.

1. Introduction

Properties of QCD matter at large energy densities are studied in high energy heavy ion collisions. The energy density of the medium can be deduced from the transverse energy per participant nucleon. The transverse energy in nucleus-nucleus collisions is generated by the initial scattering of the partonic constituents of the incoming nuclei and by reinteractions among the produced partons and hadrons. The highest collision energy measurements before the start of LHC are from the Relativistic Heavy Ion Collider (RHIC) [1, 2, 3].

2. Method

The ALICE detector [4] has precision tracking detectors and electromagnetic calorimeters. Transverse energy, E_{T}, can be measured by using the calorimeters alone [5, 1], using the tracking detectors alone, or by using the tracking detectors to measure $\pi^{\pm}$, K$^{\pm}$, p and $\bar{\mathrm{p}}$ and the electromagnetic calorimeters to measure E_{T} from e$^{\pm}$ and γ [2]. In the hybrid method E_{T} is broken into two parts, a hadronic component and an electromagnetic component:

$$E_{\mathrm{T}} = E_{\mathrm{T}}^{\mathrm{had}} + E_{\mathrm{T}}^{\mathrm{em}}. \quad (1)$$

Figure 1 shows which particles are included in the definitions of $E_{\mathrm{T}}^{\mathrm{had}}$ and $E_{\mathrm{T}}^{\mathrm{em}}$ and which contribute to the background schematically. $E_{\mathrm{T}}^{\mathrm{had}}$, which we focus on here, is defined to be the transverse energy from charged hadrons directly measured by the tracking detectors ($\pi^{\pm}$, K$^{\pm}$, p and $\bar{\mathrm{p}}$), neutral hadrons which decay through charged hadrons (Λ, $\bar{\Lambda}$, and K$^0_{\mathrm{S}}$), and neutral hadrons which are not detected efficiently by either the tracking detectors or the electromagnetic calorimeter (K$^0_{\mathrm{L}}$, n, and $\bar{\mathrm{n}}$).

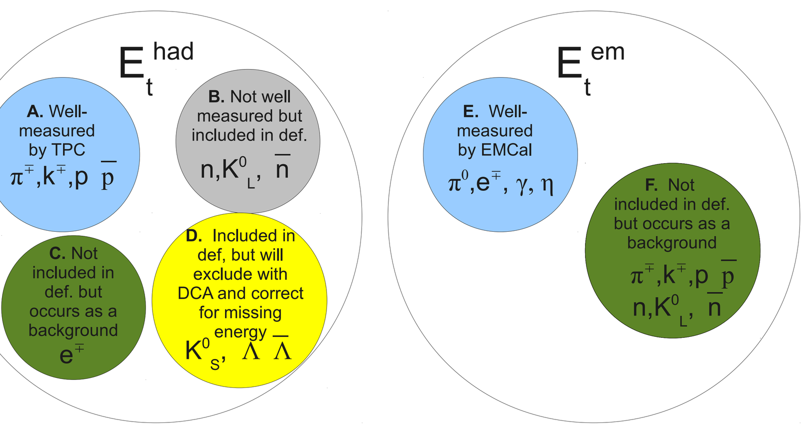

Figure 1: *Graphical depiction of the definition of $E_{\mathrm{T}}^{\mathrm{had}}$ and $E_{\mathrm{T}}^{\mathrm{em}}$*

Adhering to the traditional custom in E_{T} analyses, a particle's E_{T} is defined to be what would be measured by an ideal calorimeter:

$$E_{\mathrm{T}} = \begin{cases} \left(\sqrt{p^2+m_0^2} - m_0\right)\sin(\theta) & \text{for nucleons} \\ \left(\sqrt{p^2+m_0^2} + m_0\right)\sin(\theta) & \text{for anti-nucleons} \\ \sqrt{p^2+m_0^2}\sin(\theta) & \text{otherwise.} \end{cases} \quad (2)$$

$E_{\mathrm{T}}^{\mathrm{had}}$, with correction factors, is given by:

$$E_{\mathrm{T}}^{\mathrm{had}} = \frac{1}{f_{\mathrm{acc}}}\frac{1}{f_{p_{\mathrm{T}\mathrm{cut}}}}\frac{1}{f_{\mathrm{neutral}}}\frac{1}{f_{\mathrm{notID}}}\sum_{i=0}^{n} f_{\mathrm{bg}}^{\mathrm{i}}(p_{\mathrm{T}})\frac{1}{\mathrm{eff}(p_{\mathrm{T}}^{\mathrm{i}})}E_{\mathrm{i}}\sin(\theta^{\mathrm{i}}). \quad (3)$$

where the correction factors are:

- f_{acc}: Correction for geometric acceptance
- $f_{p_{\mathrm{Tcut}}}$: Correction for finite acceptance at low p_{T}
- f_{neutral}: Correction for hadrons not measured by tracking detectors (Λ, $\bar{\Lambda}$, K^0_{S}, K^0_{L}, n, and $\bar{\mathrm{n}}$)
- f_{notID}: Correction for $\pi^{\pm}$, K$^{\pm}$, p and $\bar{\mathrm{p}}$ which cannot be identified through dE/dx
- $f_{\mathrm{bg}}^{\mathrm{i}}(p_{\mathrm{T}})$: Correction for Λ, $\bar{\Lambda}$, and K$^0_{\mathrm{S}}$ daughters and e$^{\pm}$
- $\mathrm{eff}(p_{\mathrm{T}}^{\mathrm{i}})$: Correction for tracking efficiency

A slight modification to Equation 3 where f_{total} replaces f_{neutral} gives a hadronic measurement of the total E_{T}. f_{total} then also accounts for π^0, ω, η, e$^{\pm}$ and γ. In this analysis Time Projection Chamber (TPC) and Inner Tracking System (ITS) are used for tracking and their full acceptance is used, leading to f_{acc} =1.

2.1 Momentum acceptance $f_{p_{\mathrm{Tcut}}}$

Tracks are not reconstructed efficiently in the TPC below 150 MeV/c. A correction for this effect is determined using HIJING simulations. To determine the systematic error on this cut-off, two scenarios are considered, the case where all particles below the cut-off have a momentum of zero and the case where all particles below the cut-off have a momentum of the momentum cut-off, as in [2]. This gives $f_{p_{\mathrm{Tcut}}}$ = 0.971 ± 0.006.

2.2 Neutral particles f_{neutral}

f_{neutral} corrects for particles included in the definition of $E_{\mathrm{T}}^{\mathrm{had}}$ but not directly measured by the TPC. This is dominated by Λ, $\bar{\Lambda}$, K^0_{S}, K^0_{L}, n, and $\bar{\mathrm{n}}$. Models dramatically underpredict the contribution from Λ, $\bar{\Lambda}$, and K$^0_{\mathrm{S}}$ even for pp collisions [6], so Monte Carlo generators cannot reliably be used to determine this correction, which instead was determined by calculating the E_{T} from data in pp collisions at $\sqrt{s}$ = 900 GeV using fits to the Levy function in [6, 7].

Three approximations are made:

$$E_{\mathrm{T}}^{\mathrm{n}} = E_{\mathrm{T}}^{\mathrm{p}};\, E_{\mathrm{T}}^{\bar{\mathrm{n}}} = E_{\mathrm{T}}^{\bar{\mathrm{p}}};\, E_{\mathrm{T}}^{\mathrm{K^0_L}} = E_{\mathrm{T}}^{\mathrm{K^0_S}}. \quad (4)$$

With these approximations:

$$f_{\mathrm{neutral}} = \frac{E_{\mathrm{T}}^{\mathrm{p}} + E_{\mathrm{T}}^{\bar{\mathrm{p}}} + E_{\mathrm{T}}^{\mathrm{K}^{\pm}} + E_{\mathrm{T}}^{\pi^{\pm}}}{2E_{\mathrm{T}}^{\mathrm{K^0_S}} + E_{\mathrm{T}}^{\Lambda} + E_{\mathrm{T}}^{\bar{\Lambda}} + 2E_{\mathrm{T}}^{\mathrm{p}} + 2E_{\mathrm{T}}^{\bar{\mathrm{p}}} + E_{\mathrm{T}}^{\mathrm{K}^{\pm}} + E_{\mathrm{T}}^{\pi^{\pm}}}. \quad (5)$$

In addition, baryon enhancement has been observed for both strange [8] and non-strange [9] particles in A+A collisions, along with strangeness enhancement [10, 11]. To take these effects into account, p_{T}-dependent factors to match the RHIC data (until LHC/ALICE data are available) were applied to the spectra to determine the impact of baryon and strangeness enhancement. The value of f_{neutral} in pp collisions and the value of f_{neutral} with baryon and strangeness enhancement applied were averaged and the difference assigned as the systematic error, giving f_{neutral} = 0.69±0.05. With the assumption that $E_{\mathrm{T}}^{\pi^0} \approx \frac{1}{2}E_{\mathrm{T}}^{\pi^{\pm}}$, and using Monte Carlo generators to determine that 91% of all $E_{\mathrm{T}}^{\mathrm{em}}$ is in π^0, f_{total} = 0.55±0.02.

2.3 Particle Identification f_{notID}

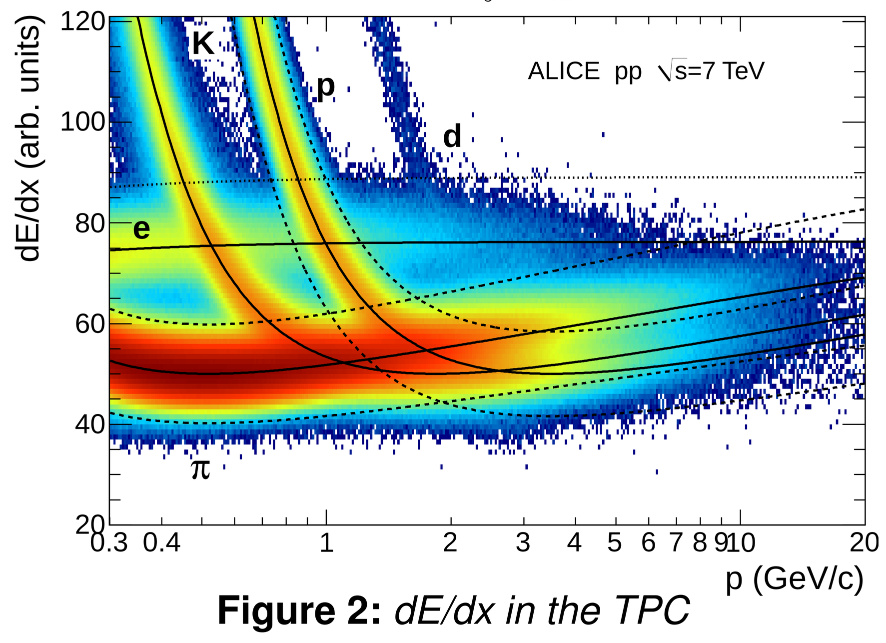

Figure 2: *dE/dx in the TPC*

Particles are identified using the dE/dx particle bands from the TPC, shown in Figure 2, in momentum regions where the bands do not overlap, and otherwise assigned as $\pi^{\pm}$. The number of particles misidentified using this algorithm is negligible. The correction for the assumption that particles that are not K$^{\pm}$, p, $\bar{\mathrm{p}}$, or electrons are assigned as pions is f_{notID}. This was calculated using Levy fits to 900 GeV p+p data assuming that all particles identifed as K$^{\pm}$, p, $\bar{\mathrm{p}}$, or electrons are identified correctly. The effects of baryon and strangeness enhancement were considered as in Section 2.2 to determine the systematic error, giving f_{notID} = 0.976±0.022.

2.4 Background $f_{\mathrm{bg}}^{\mathrm{i}}(p_{\mathrm{T}})$

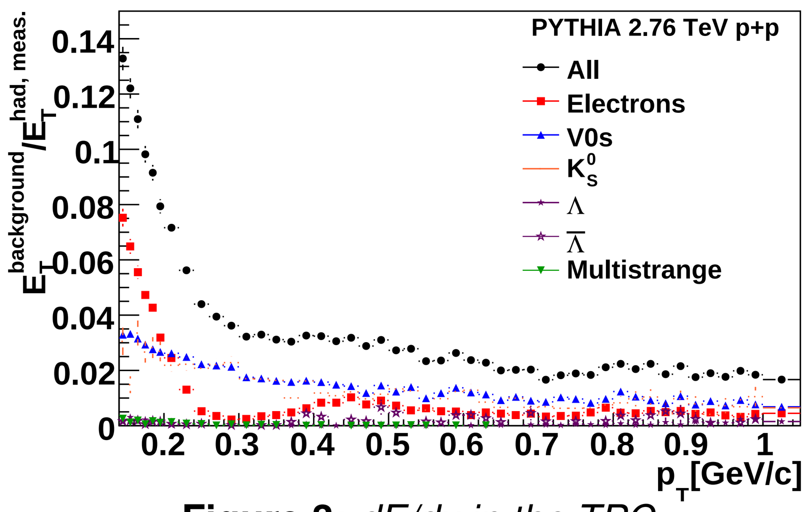

Figure 3: *dE/dx in the TPC*

Decay daughters from Λ, $\bar{\Lambda}$, and K$^0_{\mathrm{S}}$ (V^0) misidentified as primary particles and conversion electrons contribute to a background in $E_{\mathrm{T}}^{\mathrm{had}}$. PYTHIA simulations are used to determine the background contribution from V^0 daughters, rescaling the data by factors to match the data at $\sqrt{s}$ = 900 [6] and 7 TeV [12]. In addition, factors to determine the effects of baryon enhancement are applied. The average is used as the nominal value and the range is applied as a systematic error. The values from HIJING simulations are contained in this range. An example showing the contribution to the background as a function of the particle's momentum is shown in Figure 3. The contribution from conversion electrons is also determined using Monte Carlo simulations and the systematic errors on this contribution are determined by varying the material budget by 10%. These effects lead to a systematic error of 0.8% due to the background correction

2.5 Efficiency $\mathrm{eff}(p_{\mathrm{T}}^{\mathrm{i}})$

The efficiency correction is determined using HIJING simulations. The systematic error on this correction is determined by varying the material budget by 10%, leading to a systematic error of 1%.

2.6 Monte Carlo Cross Check

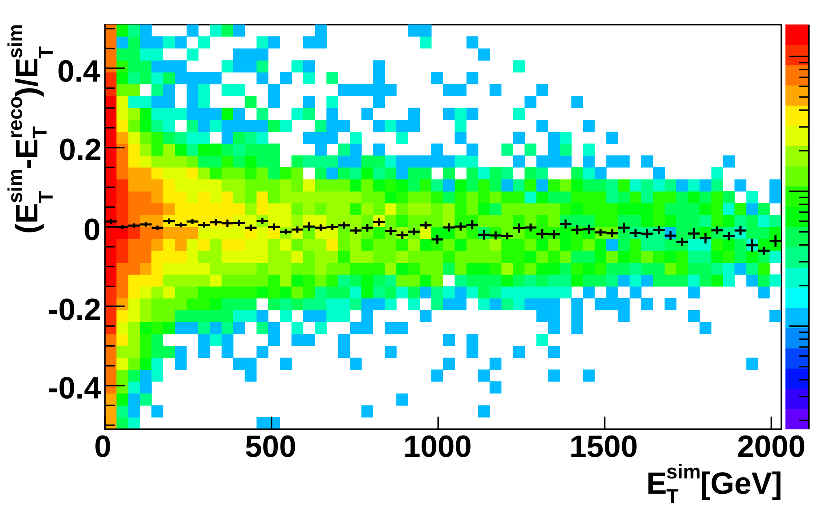

Figure 4: $(E_{\mathrm{T}}^{\mathrm{sim}} - E_{\mathrm{T}}^{\mathrm{reco}})/E_{\mathrm{T}}^{\mathrm{sim}}$ *versus* $E_{\mathrm{T}}^{\mathrm{sim}}$ *from HIJING*

Cross checks were perfomed using HIJING with f_{notID} and f_{neutral} determined from HIJING. Figure 4 shows the difference between the simulated and reconstructed $E_{\mathrm{T}}^{\mathrm{had}}$ as a function of $E_{\mathrm{T}}^{\mathrm{had}}$, demonstrating that the method effectively reconstructs $E_{\mathrm{T}}^{\mathrm{had}}$.

3. Results

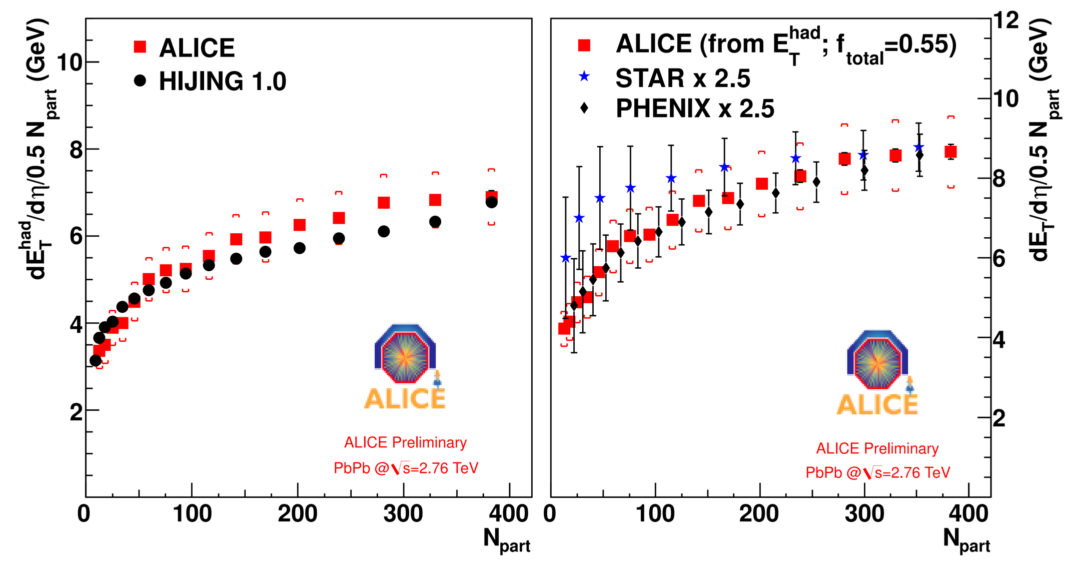

Figure 5: N_{part} *dependence of* $\langle dE_{\mathrm{T}}^{\mathrm{had}}/d\eta\rangle/(0.5\times N_{\mathrm{part}})$ *(left) and* $\langle dE_{\mathrm{T}}/d\eta\rangle/(0.5\times N_{\mathrm{part}})$ *(right)*

$E_{\mathrm{T}}^{\mathrm{had}}$ is shown in Figure 5 as a function of N_{part} in Pb–Pb collisions at $\sqrt{s_{\mathrm{NN}}}$ = 2.76 TeV and compared to results for HIJING with default settings without quenching and with a minimum p_{T} cut-off of 2.3 GeV/c.As described earlier, by replacing f_{neutral} with f_{total} we can also estimate the total E_{T}. E_{T} compared to results in Au–Au collisions at $\sqrt{s_{\mathrm{NN}}}$ = 200 GeV from STAR [2] and PHENIX [5] scaled by a factor of 2.5 are also shown in Figure 5, showing that the shape as a function of N_{part} is comparable at both energies. The result for the most central collisions is shown in Figure 6 and compared to data from lower energies (compiled in [5]) and theory predictions.

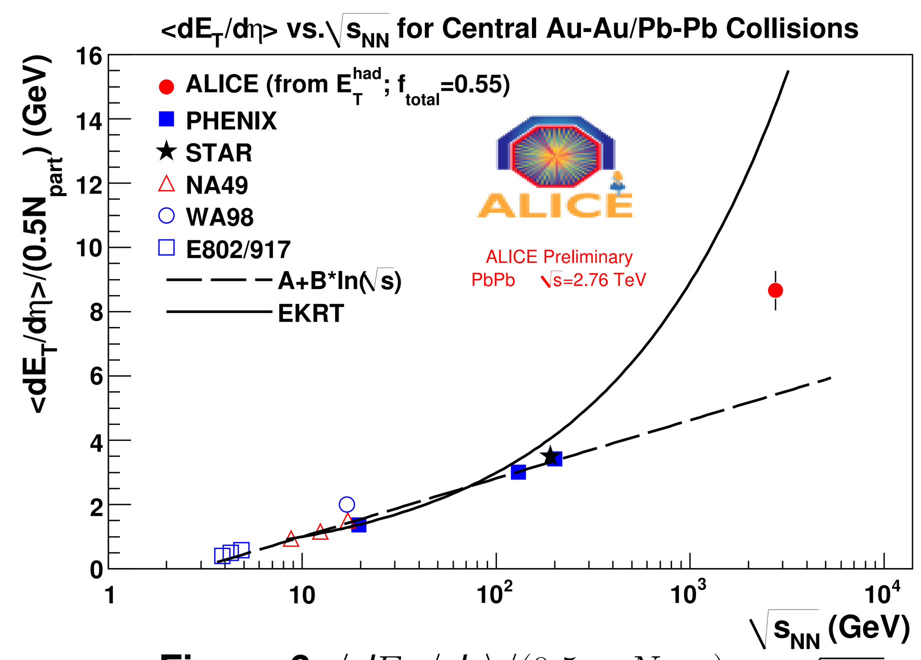

Figure 6: $\langle dE_{\mathrm{T}}/d\eta\rangle/(0.5\times N_{\mathrm{part}})$ *vs* $\sqrt{s_{\mathrm{NN}}}$

$\langle dN_{\mathrm{ch}}/d\eta\rangle/(0.5\times N_{\mathrm{part}})$ increased by a factor of about 2.1 [13] from central Au+Au at 200 GeV to central Pb–Pb at 2.76 TeV. In $\langle dE_{\mathrm{T}}/d\eta\rangle/(0.5\times N_{\mathrm{part}})$ we see an increase of about a factor 2.5±0.2, from 200 GeV to 2.76 TeV, consistent with the observed increase in $\langle p_{\mathrm{T}}\rangle$ by about 25%. Neglecting any differences between RHIC and LHC $\sqrt{s_{\mathrm{NN}}}$ values in transverse overlap area A and the conversion between dE_{T}/dy and dE_{T}/dη, the Bjorken energy density ϵ_{Bj} (multiplied by the formation time τ) increase is proportional to the dE_{T}/dη increase. With N_{part} changing from a value of 353 at RHIC to 383 at LHC, we thus arrive at an increase in $\epsilon_{\mathrm{Bj}}\times\tau$ of at least a factor 2.7±0.2 from RHIC to LHC. Since τ is expected to decrease from RHIC to LHC we can say that ϵ_{Bj} should increase by at least a factor 3 for the $\sqrt{s_{\mathrm{NN}}}$ increase from 200 GeV to 2.76 TeV.

It is more of a challenge for models to describe E_{T} than N_{ch} since E_{T} depends not only on the number of particles but also on the particle composition and momentum distributions. We compare here the E_{T} results with models that were cited in the N_{ch} analyses [13]. Several models (e.g. Albacete [14] which agrees with EKRT [15] shown in Figure 6) predict a stronger increase in $\langle dE_{\mathrm{T}}/d\eta\rangle$ at LHC energies than observed in the data. A more recent publication by Renk et al. [16] is closer to the data (≈20% above), and HIJING describes the data rather well. Future analyses when the $E_{\mathrm{T}}^{\mathrm{had}}$ and $E_{\mathrm{T}}^{\mathrm{em}}$ parts are both measured together should be able to offer stronger constraints and discriminate better between the models.

References

[1] K. Adcox *et al.*, "Measurement of the mid-rapidity transverse energy distribution from s(N N)**(1/2) = 130-GeV Au + Au collisions at RHIC," *Phys. Rev. Lett.*, vol. 87, p. 052301, 2001.

[2] J. Adams *et al.*, "Measurements of transverse energy distributions in Au + Au collisions at s(NN)**(1/2) = 200-GeV," *Phys. Rev.*, vol. C70, p. 054907, 2004.

[3] K. Adcox *et al.*, "Formation of dense partonic matter in relativistic nucleus nucleus collisions at RHIC: Experimental evaluation by the PHENIX collaboration," *Nucl. Phys.*, vol. A757, pp. 184–283, 2005.

[4] K. Aamodt *et al.*, "The ALICE experiment at the CERN LHC," *JINST*, vol. 3, p. S08002, 2008.

[5] S. S. Adler *et al.*, "Systematic studies of the centrality and s(NN)**(1/2) dependence of dE(T)/d mu and d N(ch)/d mu in heavy ion collisions at mid-rapidity," *Phys. Rev.*, vol. C71, p. 034908, 2005.

[6] K. Aamodt *et al.*, "Strange particle production in proton-proton collisions at sqrt(s) = 0.9 TeV with ALICE at the LHC," *Eur. Phys. J.*, vol. C71, p. 1594, 2011.

[7] K. Aamodt *et al.*, "Production of pions, kaons and protons in pp collisions at sqrt(s)= 900 GeV with ALICE at the LHC," 2011.

[8] M. A. C. Lamont, "Recent results on strangeness production at RHIC," *J. Phys. Conf. Ser.*, vol. 50, pp. 192–200, 2006.

[9] B. I. Abelev *et al.*, "Systematic Measurements of Identified Particle Spectra in pp, d^+ Au and Au+Au Collisions from STAR," *Phys. Rev.*, vol. C79, p. 034909, 2009.

[10] S. S. Adler *et al.*, "Identified charged particle spectra and yields in Au + Au collisions at s(NN)**(1/2) = 200-GeV," *Phys. Rev.*, vol. C69, p. 034909, 2004.

[11] A. Adare *et al.*, "Identified charged hadron production in p+p collisions at sqrt(s)=200 and 62.4 GeV," 2011.

[12] C. Collaboration, "Strange particle production in pp collisions at sqrt(s) = 0.9 and 7 TeV." CMS Analysis Note, 2010.

[13] K. Aamodt *et al.*, "Centrality dependence of the charged-particle multiplicity density at mid-rapidity in Pb-Pb collisions at sqrt(sNN) = 2.76 TeV," *Phys. Rev. Lett.*, vol. 106, p. 032301, 2011.

[14] J. L. ALbacete and A. Dumitru, "A model for gluon production in heavy-ion collisions at the LHC with rcBK unintegrated gluon densities," 2010.

[15] K. J. Eskola, P. V. Ruuskanen, S. S. Rasanen, and K. Tuominen, "Multiplicities and transverse energies in central A A collisions at RHIC and LHC from pQCD, saturation and hydrodynamics," *Nucl. Phys.*, vol. A696, pp. 715–728, 2001.

[16] T. Renk, H. Holopainen, R. Paatelainen, and K. J. Eskola, "Systematics of the charged-hadron pT spectrum and the nuclear suppression factor in heavy-ion collisions from sqrts=200 GeV to sqrts =2.76 TeV," 2011.